https://doi.org/10.32604/zkg.2026.075750

ARTICLE

Corrosion protection performance of magnesium phosphate cement for steel bar exposed to carbonation and chlorides

Hanxin Li[1,2], Zhicheng Zhang[1], Changkun Song[1], Junzhe Liu[1] and Songyuan Ni[1,2,*]
[1]School of Architectural Engineering, Qingdao Agricultural University, Qingdao, China
[2]Harbin Institute of Technology (Weihai) Qingdao Research Institute, Qingdao, China
*Corresponding Author: Songyuan Ni. Email: nisy@qau.edu.cn

Received: 07 November 2025; Accepted: 06 February 2026

ABSTRACT: This study investigates the impact of carbonation and chloride penetration on the corrosion of steel bars embedded in magnesium phosphate cement. Specimens with varying chloride concentrations (0%, 1%, 2%, and 3%) were prepared and cured under both natural and carbonation conditions. A combination of macroscopic tests and electrochemical techniques, along with microstructural analysis, was used to examine the corrosion behavior. The results show that increased chloride content weakens the corrosion protection of the steel bars, with carbonation accelerating this degradation. In natural curing conditions, corrosion began when the chloride level reached 2%, while carbonation reduced this threshold to 1%. The microstructural analysis revealed that higher chloride content caused cracks in the protective film on the steel surface, weakening the bond between the steel and the surrounding material, thus diminishing the overall protection of the reinforcement.

KEYWORDS: Magnesium phosphate cement; carbonation; chloride ions; steel bars corrosion

1 Introduction

Magnesium phosphate cement (MPC) has attracted increasing attention as a rapid-hardening, high-early-strength, and chemically stable repair material for deteriorated reinforced concrete (RC) structures, particularly in marine and coastal environments [1–3]. Unlike ordinary Portland cement (OPC), MPC hydrates through the reaction between dead-burned MgO and phosphate, forming mainly struvite-type products with dense microstructures, low alkalinity, and good adhesion to existing substrates [4, 5]. These characteristics make MPC a promising candidate for steel bar protection in patch repairs, emergency strengthening, and localized corrosion control where fast return-to-service and durable bonding are required.

However, RC structures in service are often subjected to multiple deterioration factors simultaneously, among which carbonation and chloride ingress are two of the most critical [6, 7]. Carbonation lowers the pore solution pH and weakens the passivity of embedded steel [8, 9], whereas chlorides can promote localized (pitting) corrosion even in alkaline environments [10, 11]. For MPC systems, whose pore solution pH is inherently lower than that of OPC, the combined action of carbonation and chlorides may be more detrimental, shortening the incubation period and hastening the propagation phase.

Existing studies have confirmed that phosphate species in MPC can interact with Fe^{2+}/Fe^{3+} to form protective, phosphate-containing films on the steel surface, thereby improving corrosion resistance compared with OPC matrices. Zhang et al. performed accelerated corrosion tests on MPC slurry applied to ribbed mild steel bars, showing that the MPC slurry coating exhibited stable impedance development and provided significantly better protection than OPC [12]. Tang et al. investigated the electrochemical behavior of steel bars in MPC, revealing its passivation mechanism and determining the corrosion protection mechanism of MPC for steel bars using techniques such as Environmental Scanning Electron Microscopy (ESEM) and X-ray Photoelectron Spectroscopy (XPS), with results indicating that MPC's hydration products effectively prevent the initiation and propagation of steel bars corrosion [13–15]. Additionally, research on the resistance of steel bars to carbonation corrosion in MPC cement has also been explored. Wang et al. examined the corrosion performance and mechanism of steel bars in MPC slurries, concluding that carbonation reduces corrosion in low-M/P slurries by promoting the formation of ferrous oxide and iron phosphate/ferric borate, which enhances the protective ability of the oxide film [16].

While existing research primarily focuses on the individual effects of chloride ion corrosion

MATERIALS

or carbonation, the combined impact of seawater mixing and carbonation on MPC concrete remains underexplored. Therefore, the present study focuses on the corrosion protection performance of the steel bars of magnesium phosphate cement under simultaneous carbonation and chloride exposure. By preparing MPC specimens with different chloride contents and subjecting them to natural and accelerated carbonation, the work evaluates corrosion initiation and propagation using electrochemical tests (Natural potential, EIS, and LPR), macroscopic corrosion assessments (corrosion area and mass loss), and microstructural characterization (ESEM-EDS). The objective is to reveal how chloride level and carbonation jointly affect the integrity of the phosphate-derived passive film and the steel-matrix interface, and to provide a mechanistic basis for designing MPC repair materials with enhanced durability in marine and CO_2-rich service environments.

2 Materials and methods

2.1 Materials

Magnesium phosphate cement (MPC) was prepared using dead-burned magnesia (MgO), potassium dihydrogen phosphate (KDP), and borax as a retarder. Based on prior studies, a mix proportion that ensures superior steel bar protection performance and relatively stable electrochemical behavior was adopted. The Mg-to-phosphate ratio (M/P) was set at 4:1, and borax was added at 12 wt% of MgO. The MgO used was calcined at 1600°C, with a density of 3.48 g/cm³ and a specific surface area of 225 m²/kg, with its chemical composition detailed in Table 1. Industrial-grade KDP was used as the phosphate source, while sodium borate ($Na_2B_4O_7{\cdot}10H_2O$) acted as the retarder. Chloride ions were introduced into the specimens using analytical-grade NaCl reagent. All components were thoroughly dry-mixed to form the MPC. The steel substrate used in this study was carbon steel, and the steel bars were plain round bars with a diameter of 8 mm; their elemental composition is shown in Table 2.

Table 1 **Chemistry of dead-burned magnesia**

MgO	SiO_2	CaO	Fe_2O_3	Others
87.36	5.32	4.85	0.81	1.66

Table 2 **Main chemical elements of steel bars**

C	Si	Mn	P	S	Fe
0.24	0.24	0.73	0.023	0.019	Bal.

2.2 Preparation of specimen

The tests were conducted using HPB300 smooth round steel bars with a diameter of 8 mm and lengths of 398 mm, 80 mm, 2 mm, respectively. Before embedding the steel bars into the concrete specimens, they were treated to remove surface contaminants. This treatment involved immersing the steel bars in a 10% ammonium citrate solution for 7 days. After the treatment, the steel bars were taken out, thoroughly rinsed to remove any remaining ammonium citrate solution, and dried with a towel. The bars were placed in an oven at approximately 60°C for drying then. After drying, the steel bars were polished sequentially with 400, 500, and 600 mesh sandpaper until a bright finish was attained. Finally, the polished steel bars were wrapped in parafilm and prepared for use in the experimental setup. The treated steel bar specimens are shown in Figure 1.

The preparation of specimens for the Natural potential test, steel bar corrosion area ratio, and mass loss rate was carried out as follows: Wooden boards measuring 98 mm × 98 mm × 10 mm were placed at both ends of a 400 mm × 100 mm × 100 mm mold for positioning and supporting. A φ8 mm × 398 mm steel bar was then securely fixed in the mold using the boards to ensure accurate positioning and alignment after which, the concrete was cast. The schematic is shown in Figure 2a.

The preparation of electrochemical test specimens was as follows: Fresh cement paste was cast into steel cubic molds (70 mm × 70 mm × 70 mm). After standing for 10 min, two bar-type elements were embedded sequentially—a deformed steel bar (φ8 mm × 80 mm) and a stainless-steel wire mesh panel (65 mm × 65 mm × 80 mm) arranged parallel to one face of the specimen. After demolding, the exposed portion of the steel bar was encapsulated with epoxy resin immediately, and the specimens were cured under controlled laboratory conditions (25 ± 2°C, RH 60% ± 5%). The mix proportions of the neat cement paste are provided in Table 3. The schematic of the electrochemical specimen is shown in Figure 2c.

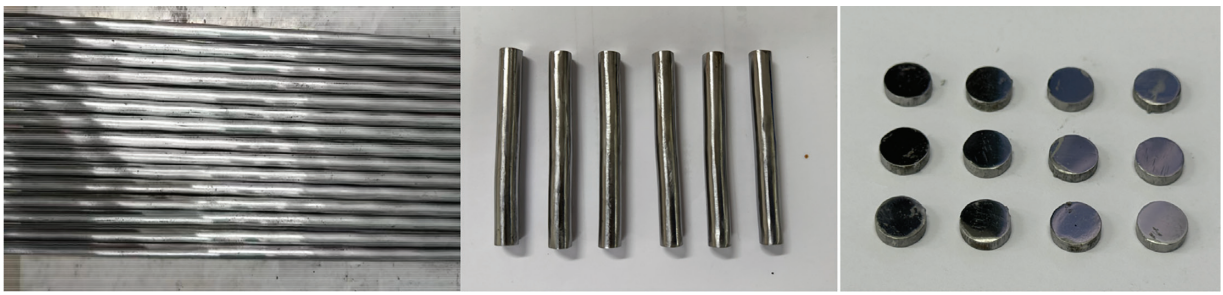

Figure 1 **Polished steel bars specimen**

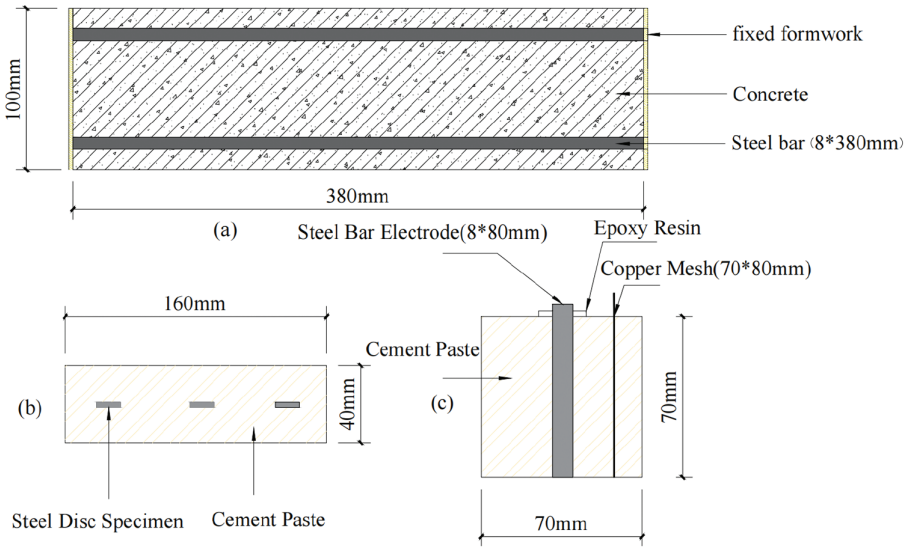

Figure 2 Schematic of the test specimen. (a) natural potential test; (b) Micro test; (c) electrochemical test

Table 3 Mixture Proportions of MPC Concrete (kg/m³)

No.	MgO	KDP	NaCl	H_2O	Borax	Sand	Gravel	Curing method
NC-0	387.03	325.24	0	139.33	46.44	643.58	1216.38	Natural curing
NC-1	387.03	325.24	6.38	139.33	46.44	643.58	1216.38	
NC-2	387.03	325.24	12.76	139.33	46.44	643.58	1216.38	
NC-3	387.03	325.24	19.14	139.33	46.44	643.58	1216.38	
TC-0	387.03	325.24	0	139.33	46.44	643.58	1216.38	carbonation curing
TC-1	387.03	325.24	6.38	139.33	46.44	643.58	1216.38	
TC-2	387.03	325.24	12.76	139.33	46.44	643.58	1216.38	
TC-3	387.03	325.24	19.14	139.33	46.44	643.58	1216.38	

Table 4 Mixture Proportions of magnesium phosphate cement (kg/m³)

No.	MgO	KDP	NaCl	Borax	H_2O	Curing method
NCP-0	313.46	263.42	0.00	37.61	112.85	Natural curing
NCP-1	313.46	263.42	5.17	37.61	112.85	
NCP-2	313.46	263.42	10.33	37.61	112.85	
NCP-3	313.46	263.42	15.50	37.61	112.85	
TCP-0	313.46	263.42	0.00	37.61	112.85	carbonation curing
TCP-1	313.46	263.42	5.17	37.61	112.85	
TCP-2	313.46	263.42	10.33	37.61	112.85	
TCP-3	313.46	263.42	15.50	37.61	112.85	

Freshly mixed cement paste was cast into molds measuring 40 mm × 40 mm × 160 mm. After resting for 5 min, steel discs were embedded in the paste at the predetermined positions (layout shown in Figure 2b). The surface was leveled, then the specimens were kept at room conditions for 1 h, demolded, and transferred to a curing chamber for 180 d. The mix proportions and specimen designations for the paste are listed in Table 4.

2.3 Test methods

The mass loss ratio (MLR, %) was calculated by measuring the initial mass of the steel bar (m_0) and the final mass after exposure (m_t), and expressing the mass loss as a percentage of the initial mass:

$$MLR\ (\%) = [(m_0 - m_t)/m_0] \times 100\% \quad (1)$$

The corrosion area ratio (CAR, %) was obtained by comparing the visually corroded area with the total surface area of the bar segment:

$$CAR\ (\%) = (A_{corr}/A_{total}) \times 100\% \quad (2)$$

For area measurement, the corroded regions on this segment were outlined with a permanent marker, and the marked surface was then transferred onto graph paper to capture the outline.

The blackened area was quantified by counting the grid squares, converting to area, and dividing by the segment's geometric surface area to calculate the CAR.

Natural potential testing was conducted in accordance with ASTM C876. The specimen surface was kept moist to maintain a continuous electrolyte path. Steel bars embedded in MPC concrete served as working electrodes and were connected to a high-input-impedance voltmeter. A saturated calomel electrode was used as the reference electrode. Measurements were recorded after the potential stabilized, with readings taken at three locations on each specimen and averaged.

Electrochemical impedance spectroscopy (EIS) and potentiodynamic polarization (Tafel) tests were conducted using an electrochemical workstation. A three-electrode configuration was employed, consisting of a working electrode, counter electrode, and reference electrode. The steel bars embedded in the MPC paste served as the working electrode, while a stainless-steel wire mesh acted as both the counter and reference electrodes. Electrochemical parameters of specimens at various ages were measured using a CHI760E multichannel electrochemical workstation. Prior to formal testing, a 20-min open-circuit potential measurement was performed to ensure the stability of the system's potential.

To gain a deeper understanding of the protective effect of MPC on steel corrosion, the surface morphology and elemental composition of the steel specimens were analyzed using Environmental Scanning Electron Microscopy-Energy Dispersive X-ray Spectroscopy (ESEM-EDS) at an accelerating voltage of 20 kV and a working distance of 15 mm.

3 Results and discussion

3.1 Macroscopic corrosion evaluation

3.1.1 Mass loss rate

The MLR of steel bars is the most direct and reliable metric for quantifying corrosion damage [17–19]. As a cumulative measure of corrosion, the WLR effectively reflects the net metal loss and can be used to calculate the average thickness loss and the reduction in cross-sectional area. Figure 3 illustrates how chloride content influences the 180-day mass loss of steel bars embedded in MPC composites under both natural and carbonated conditions. In both exposure conditions, the MLR increases monotonically with increasing chloride content. Compared to natural curing, specimens subjected to carbonation show significantly higher mass loss rates, indicating a more aggressive corrosion process and the formation of more loosely adherent (spallable) corrosion products. A sharp rise in mass loss rate occurs when the chloride content reaches or exceeds 2%, primarily because the chloride concentration reaches the critical

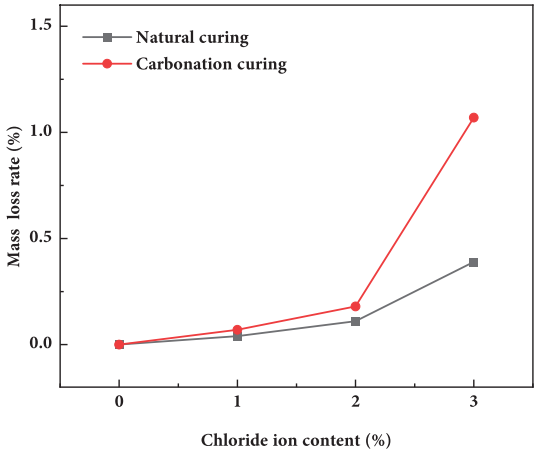

Figure 3 Mass loss rate of steel bars in concrete at different chloride ion contents

corrosion (depassivation) threshold for steel in MPC. In contrast, at 0% chloride, the MLR is negligible, demonstrating that chloride ion is the primary driver of steel corrosion in this system, with carbonation acting as a strong accelerator.

3.1.2 Corrosion area ratio

Unlike the mass loss ratio, the CAR quantifies the areal fraction of the visibly corroded surface, thus directly revealing the spatial distribution of corrosion and its degree of localization (pitting) [20, 21]. As shown in Figure 4, the evolution of the corrosion area ratio closely follows that of the MLR. Additionally, Figure 4 demonstrates that the extent of steel bar corrosion is influenced by both chloride content and carbonation: in Figure 5a, the NC-0 group (without added chloride) developed a uniform, compact film of phosphate hydration products on the steel surface, primarily attributed to struvite and iron-phosphate species [22, 23]; once corrosion occurred (e.g., TC-3), the surface became dominated by loosely adherent, reddish-brown iron oxides, tentatively identified as Fe_2O_3. A comparison of Figure 4b, 4c reveals

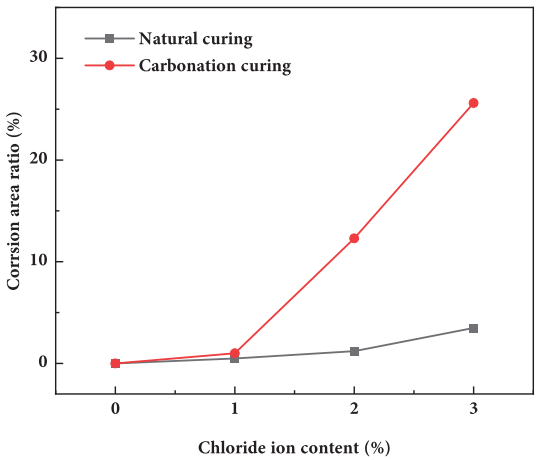

Figure 4 Corrosion area ratio at different chloride concentrations

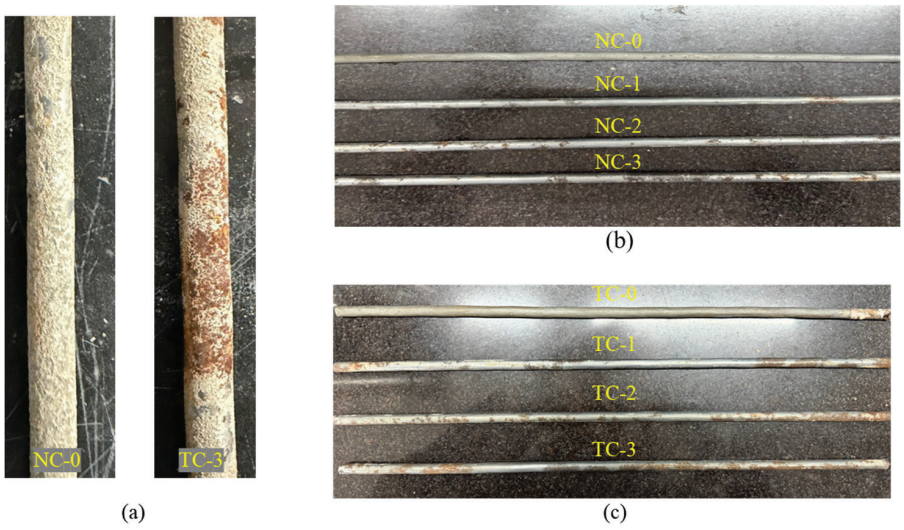

Figure 5 Corrosion morphology images of steel bars (a) local enlargement; (b) natural curing; (c) carbonation curing

that corrosion in this study was predominantly uniform, with no obvious pitting. Furthermore, for carbonated specimens, corrosion was concentrated near the ends of the bars, presumably because carbonation initiated earlier at the ends and the carbonation front propagated inward.

3.2 Electrochemical testing

3.2.1 Natural potential

Natural potential, a relatively traditional nondestructive technique, measures the potential difference resulting from the electrochemical state at the steel–pore solution interface. Due to its simplicity, rapid testing, and straightforward data interpretation, Natural potential is widely applied in both laboratory and field settings [24–26]. However, because the passivation mechanism of steel in magnesium phosphate cement (MPC) differs from that in ordinary Portland cement, existing potential-based criteria may not necessarily be applicable to MPC [27, 28]. Natural potential measurements were conducted on specimens cured for 3, 7, 14, and 28 days to evaluate the effect of chloride content on steel bar corrosion in MPC concrete (Figure 6). The results indicate that after casting, the Natural potential is low, due to the initially low pH of the MPC pore solution, the absence of a stable passive film, and relatively high ionic conductivity—indicating that the steel is in an active state. As curing progresses, the pore-solution pH increases, the phosphate-based passive film densifies, and the pore structure stabilizes; accordingly, the steel gradually passivates and the Natural potential rises toward a steady value. In the presence of chloride, the increase in Natural potential is progressively attenuated with rising chloride concentration, and carbonation further suppresses the Natural potential rise, suggesting that chloride activates the steel surface while carbonation intensifies this corrosive effect. A Comparison of Natural potential with MLR and CAR results indicates that, under the present

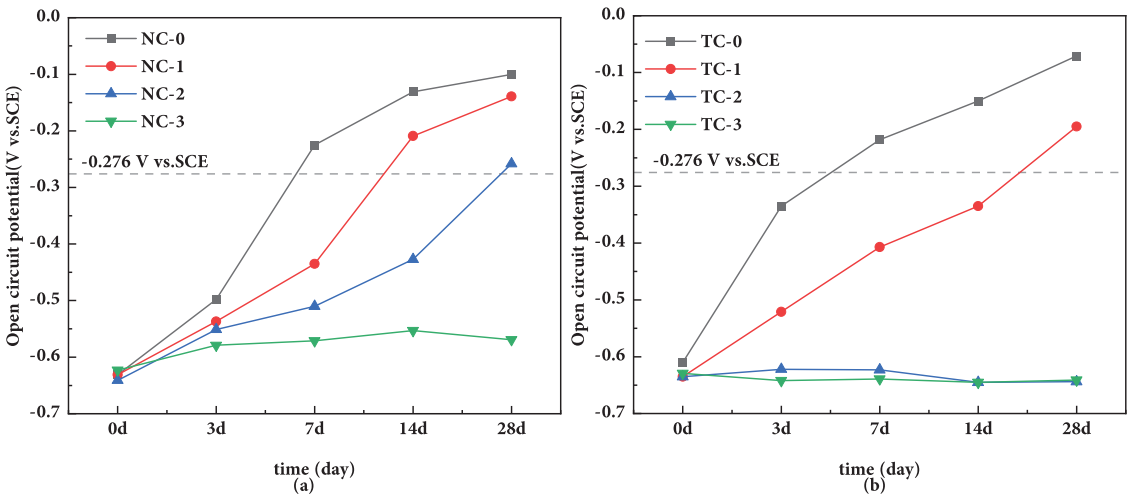

Figure 6 Spontaneous potentials of steel bars at different ages (a) natural curing; (b) carbonation curing

mix proportions and test conditions, corrosion occurred when the potential was below −0.276 V (vs SCE) [24], whereas no corrosion was observed above this threshold. This correlation supports the validity of the experimental data and suggests that, under the conditions of this study, Natural potential can serve as an effective indicator for assessing steel corrosion in MPC systems.

3.2.2 EIS results

Figure 7 presents the equivalent circuit employed in this study, obtained by fitting the EIS data with ZSimpWin. R_s denotes the pore-solution resistance of the cement paste; R_1 is the resistance of the cement-paste cover layer; R_2 represents the charge-transfer resistance of the steel corrosion reaction, i.e., the true polarization resistance; Q_1 is a constant-phase element (CPE) for the cement-paste cover layer; Q_2 is a CPE for the electrical double layer at the steel interface; and W is the diffusion-related impedance (Warburg). The frequency range of the electrochemical impedance spectroscopy is from 0.01 Hz to 100 kHz. The data after fitting with the equivalent circuit are shown in Table 5.

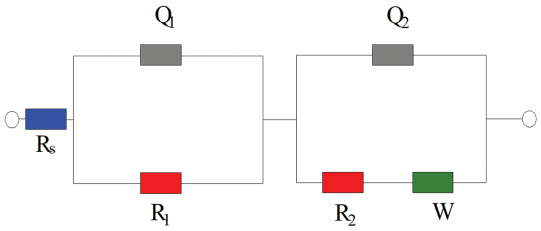

Figure 7 Equivalent circuit diagram of steel bars-MPC paste specimen

In MPC paste, under natural curing (Figure 8), as curing time increases, the Nyquist plots of the steel electrode shift markedly to the right along the real axis (Z′), indicating an increase in pore-solution/ohmic resistance. This suggests that unreacted MgO continues to react with KH_2PO_4 to form highly crystalline $MgKPO_4{\cdot}6H_2O$ (K-struvite), thereby effectively reducing conductive pathways in the hardened matrix. Additionally, when the chloride concentration is below 2%, the

Table 5 Fitting results of electrochemical impedance spectroscopy

No.	Curing time	Rs/Ω·cm²	R1/Ω·cm²	R2/Ω·cm²	Chi-squared
NCP-0	3 d	639.53	3386.15	4.684E+04	1.39E–06
	7 d	1138.64	4376.35	10.08E+04	3.27E–05
	14 d	1888.85	6374.47	11.43E+04	9.54E–06
	28 d	2156.13	6766.19	12.91E+04	1.92E–06
NCP-1	3 d	621.57	3216.84	4.496E+04	7.08E–05
	7 d	1011.90	4070.01	9.374E+04	4.61E–04
	14 d	1534.31	5832.64	10.37E+04	2.35E–05
	28 d	1869.49	6069.27	10.59E+04	8.49E–05
NCP-2	3 d	566.74	2820.82	4.133E+04	6.73E–04
	7 d	916.35	3691.61	8.46E+04	5.10E–05
	14 d	1371.28	5233.72	9.10E+04	7.54E–05
	28 d	1624.57	5510.96	9.68E+04	9.31E–05
NCP-3	3 d	531.23	3678.33	3.95E+04	9.88E–06
	7 d	551.65	3311.78	3.87E+04	7.95E–06
	14 d	654.73	3244.61	3.62E+04	3.74E–05
	28 d	745.69	3166.96	3.76E+04	4.90E–04
TCP-0	3 d	425.69	2201.07	3.04E+04	1.27E–06
	7 d	760.12	2864.63	6.55E+04	3.00E–05
	14 d	1237.75	4153.41	7.13E+04	8.74E–06
	28 d	1411.48	4338.02	8.49E+04	1.76E–06
TCP-1	3 d	414.02	2290.95	2.92E+04	6.49E–05
	7 d	657.74	2745.51	6.09E+04	4.22E–04
	14 d	997.30	3891.22	6.74E+04	2.15E–05
	28 d	1275.17	3945.03	7.78E+04	7.78E–05
TCP-2	3 d	566.74	2820.82	3.13E+04	6.16E–04
	7 d	916.35	3691.61	3.46E+04	4.67E–05
	14 d	1018.28	3233.72	3.10E+04	6.91E–05
	28 d	1024.57	3110.96	3.69E+04	8.53E–05
TCP-3	3 d	531.23	3678.85	2.95E+04	9.05E–06
	7 d	551.65	3311.35	2.87E+04	7.28E–06
	14 d	654.73	3244.93	2.66E+04	3.43E–05
	28 d	745.69	3166.16	2.76E+04	4.49E–04

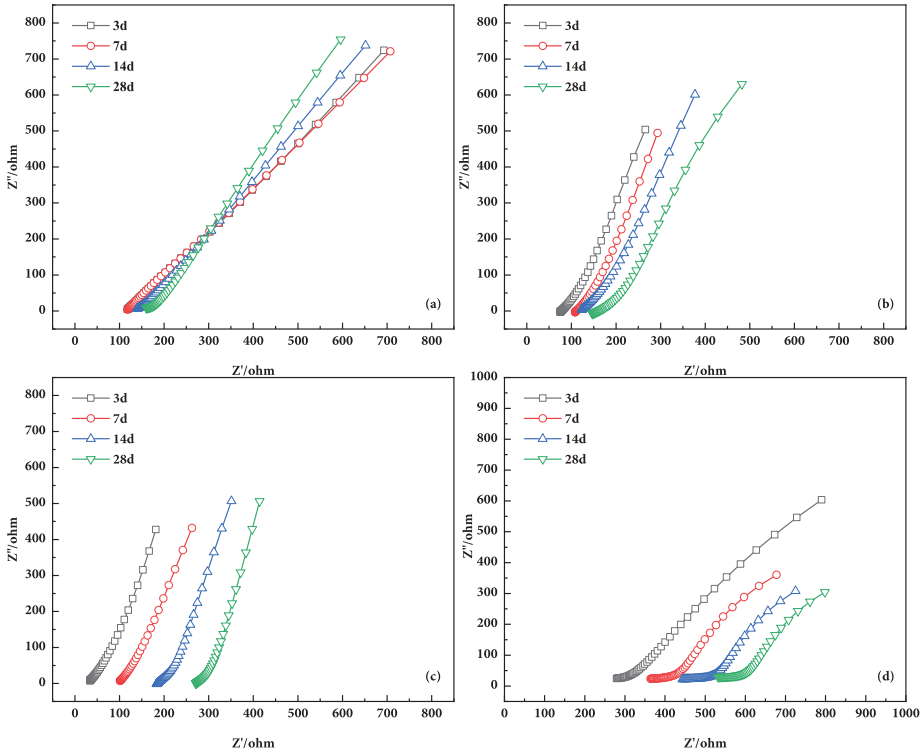

Figure 8 Nyquist plots of steel bars in MPC paste under natural curing: (a) 0% Cl^-, (b) 1% Cl^-, (c) 2% Cl^-, (d) 3% Cl^-

low-frequency slope of the Nyquist plots increases with age; the interfacial charge-transfer resistance of the steel bar is large, implying the formation of a relatively intact passive film. Although the impedance of the chloride-dosed specimens is lower than that of the chloride-free group, the steel bars still exhibit high impedance at 28 days, indicating a stable passive state. When the chloride concentration exceeds 2%, the diameter of the low-frequency capacitive semicircle in the Nyquist plot gradually decreases, indicating that the passive film exhibits low stability, poor overall passivation performance, and limited protective effect on the steel [28, 29]. Under carbonation (Figure 9), the development of steel-electrode impedance is markedly lower than that under

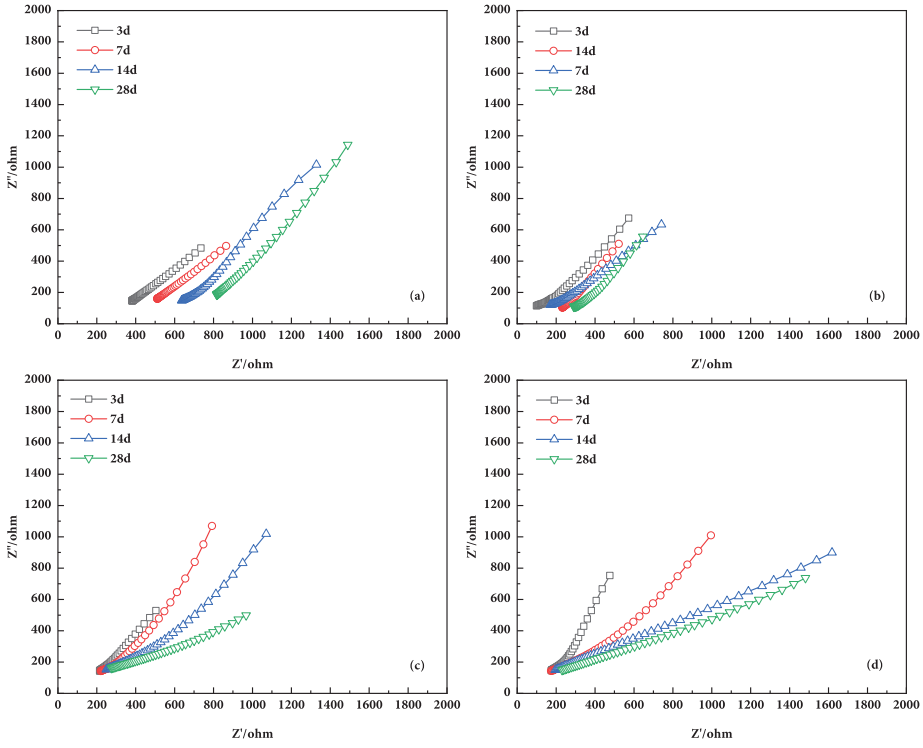

Figure 9 Nyquist plots of steel bars in MPC paste under carbonation curing: (a) 0% Cl^-, (b) 1% Cl^-, (c) 2% Cl^-, (d) 3% Cl^-

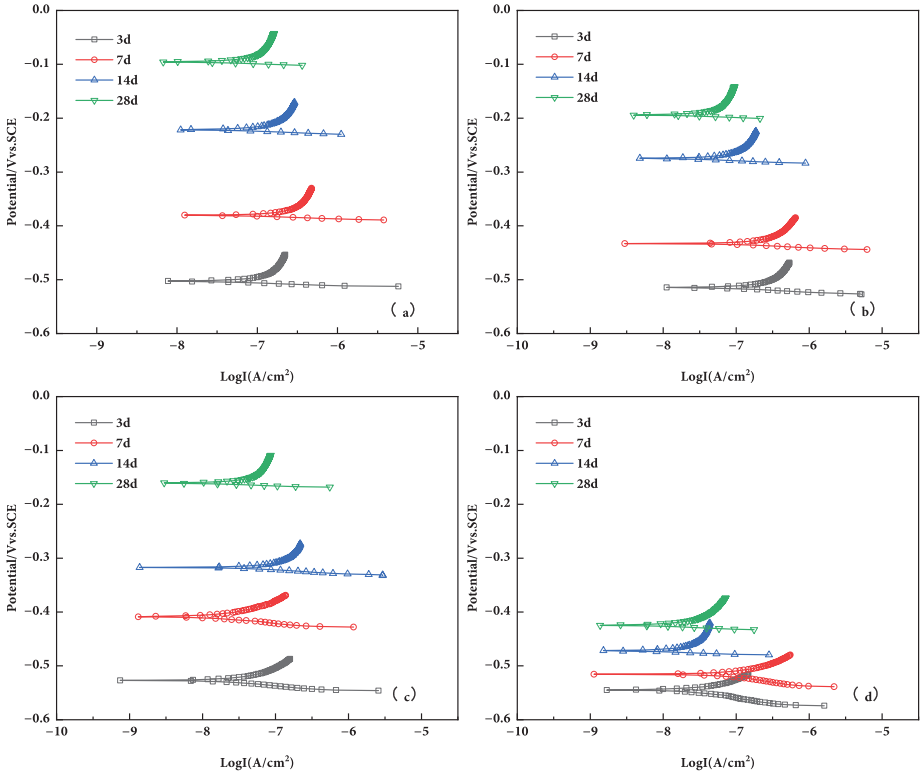

Figure 10 Tafel curves of steel bars under natural curing: (a) 0% Cl^-, (b) 1% Cl^-, (c) 2% Cl^-, (d) 3% Cl^-

natural curing at the same conditions. The low-frequency capacitive arc in the Nyquist plot disappears, being replaced by an approximately 45° inclined straight line—a typical Warburg diffusion signature [30]. This suggests a shift of the interfacial process from charge-transfer control to diffusion control and indicates that, under carbonation, reaction products and electroactive species at the steel-bar interface are continuously diffusing and migrating.

3.2.3 Tafel results

The electrochemical behavior of MPC paste cured for 3, 7, 14, and 28 days was also investigated using polarization curves. Figures 10 and 11 show the Tafel polarization curves of chloride-containing

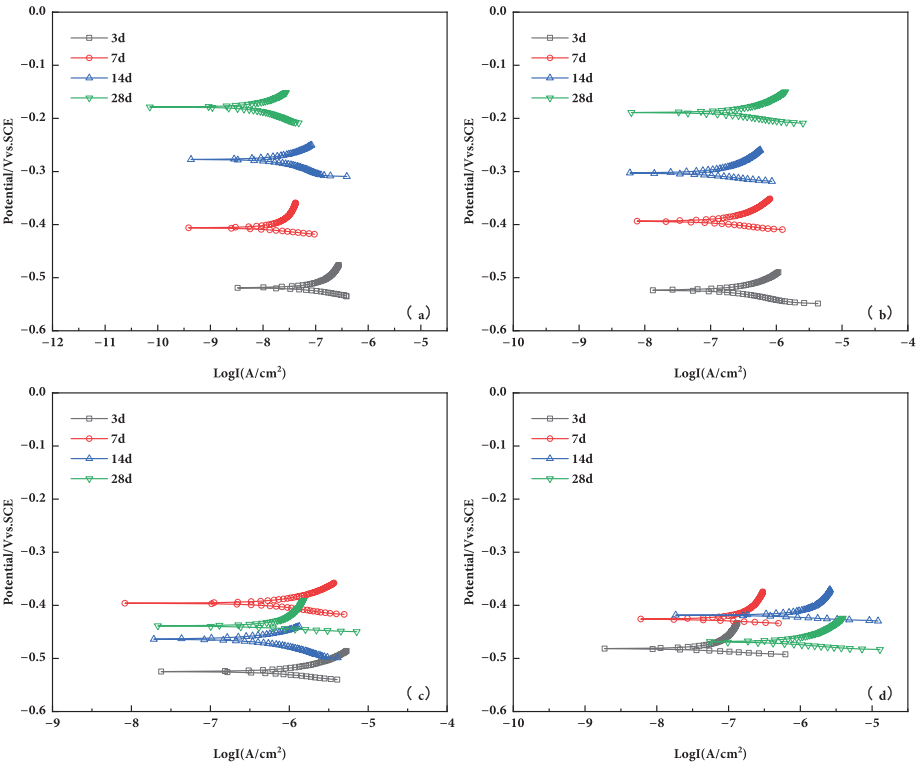

Figure 11 Tafel curves of steel bars under carbonation curing: (a) 0% Cl^-, (b) 1% Cl^-, (c) 2% Cl^-, (d) 3% Cl^-

MPC specimens under natural curing and carbonation curing conditions, respectively. According to electrochemical corrosion theory, in the vicinity of the corrosion potential E_{corr} (approximately ±10 mV), the potential–current response is linear [31]. The corrosion current density of the metal can be expressed as:

$$I_{corr} = \frac{B}{R_p} \quad (3)$$

where I_{corr} denotes the corrosion current density; R_p is the polarization resistance, i.e., the slope of the polarization curve at the corrosion potential E_{corr}; and B is a constant determined by the anodic and cathodic Tafel slopes β_a and β_c of the corrosion process, as shown in Figure 12. The specific data are shown in Table 6.

Variations in corrosion potential E_{corr} and corrosion current density provide an effective basis for evaluating the corrosion tendency and rate of steel bar [32]. As shown in Figure 11, when the chloride concentration is below 2%, the polarization curves shift with curing time toward decreasing I_{corr} and more positive E_{corr}; by 28 days, the corrosion current density at the steel surface stabilizes. Although increasing chloride raises I_{corr} and lowers E_{corr}, the values remain within a relatively steady range, indicating the gradual formation of a passive film and a progressive reduction

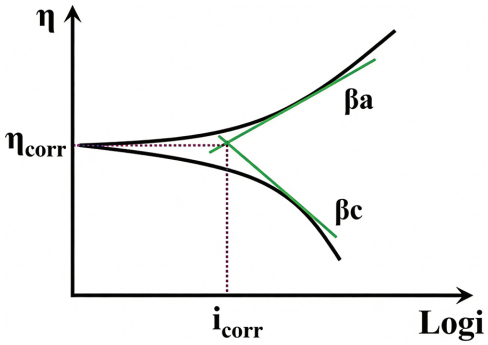

Figure 12 Schematic of the extrapolation method for determining polarization resistance

Table 6 The electrochemical parameters of MPC cement

No.	Curing time	I_{corr} (A/cm²)	E_{corr} (V)	βa (mV dec⁻¹)	βc (mV dec⁻¹)	Corrosionrate (g/m² h)
NCP-0	3 d	2.31×10^{-7}	−0.504	10.7	−198.9	0.0245
	7 d	1.55×10^{-7}	−0.379	8.8	−168.2	0.0164
	14 d	1.37×10^{-7}	−0.154	10.6	−178.0	0.0145
	28 d	7.53×10^{-8}	−0.099	6.2	−177.9	0.0797
NCP-1	3 d	5.63×10^{-7}	−0.515	23.19	−178.0	0.0596
	7 d	4.89×10^{-7}	−0.432	13.08	−121.14	0.0518
	14 d	1.59×10^{-7}	−0.176	11.92	−143.21	0.0168
	28 d	9.77×10^{-8}	−0.122	10.53	−43.64	0.1035
NCP-2	3 d	5.31×10^{-7}	−0.528	22.75	−182.37	0.0562
	7 d	3.21×10^{-7}	−0.409	19.78	−125.05	0.0340
	14 d	2.04×10^{-7}	−0.316	15.82	−50.43	0.0216
	28 d	1.52×10^{-7}	−0.161	16.35	−56.22	0.0161
NCP-3	3 d	5.04×10^{-7}	−0.546	24.01	−182.56	0.0534
	7 d	5.78×10^{-7}	−0.521	23.08	−114.85	0.0612
	14 d	5.37×10^{-7}	−0.471	17.2	−44.19	0.0569
	28 d	8.65×10^{-7}	−0.426	19.82	−47.22	0.0916
TCP-0	3 d	5.95×10^{-7}	−0.520	13.07	−188.00	0.0630
	7 d	2.31×10^{-7}	−0.408	12.48	−105.71	0.0245
	14 d	1.02×10^{-7}	−0.278	9.82	−190.50	0.0108
	28 d	9.08×10^{-8}	−0.176	8.86	−35.08	0.0962
TCP-1	3 d	7.41×10^{-7}	−0.523	18.53	−150.00	0.0785
	7 d	4.56×10^{-7}	−0.393	12.76	−140.86	0.0483
	14 d	5.31×10^{-7}	−0.303	11.91	−136.57	0.0351
	28 d	4.13×10^{-7}	−0.189	11.53	−95.76	0.0226
TCP-2	3 d	2.75×10^{-6}	−0.525	22.69	−76.91	0.0291
	7 d	1.07×10^{-6}	−0.465	20.31	−75.01	0.0113
	14 d	8.31×10^{-7}	−0.439	19.58	−59.27	0.0880
	28 d	1.38×10^{-6}	−0.394	19.34	−58.87	0.0146
TCP-3	3 d	1.91×10^{-7}	−0.525	25.51	−75.35	0.0202
	7 d	1.58×10^{-6}	−0.425	22.73	−70.68	0.0167
	14 d	2.25×10^{-6}	−0.419	23.11	−78.95	0.0238
	28 d	3.31×10^{-6}	−0.467	18.36	−61.86	0.0351

in corrosion rate. When the chloride concentration reaches 3%, the polarization curves exhibit the opposite trend: with increasing curing time, E_{corr} decreases while I_{corr} increases, suggesting instability of the passive film and a higher probability of corrosion. At the macroscale, the corrosion area ratio and mass-loss ratio at 3% chloride are 86% and 81% higher, respectively, than at 2%, which agrees with the electrochemical results. As shown in Figure 12, carbonation shifts the polarization curves overall toward more negative E_{corr} and higher I_{corr} relative to natural curing. Even without added chloride, the pH decrease induced by carbonation increases the corrosion tendency of the steel electrode; however, I_{corr} remains low and corrosion does not occur. Once the chloride concentration exceeds 1%, I_{corr} shows a pronounced upward trend compared to the naturally cured specimens. When the chloride concentration exceeds 2%, the corrosion current on the steel electrode surface remains consistently high, indicating that under carbonation conditions, the steel surface remains in an active corrosion state and has not yet reached a stable corrosion threshold.

3.3 Micro results

Figures 13 and 14 show the micro-morphology of steel discs in paste under natural and

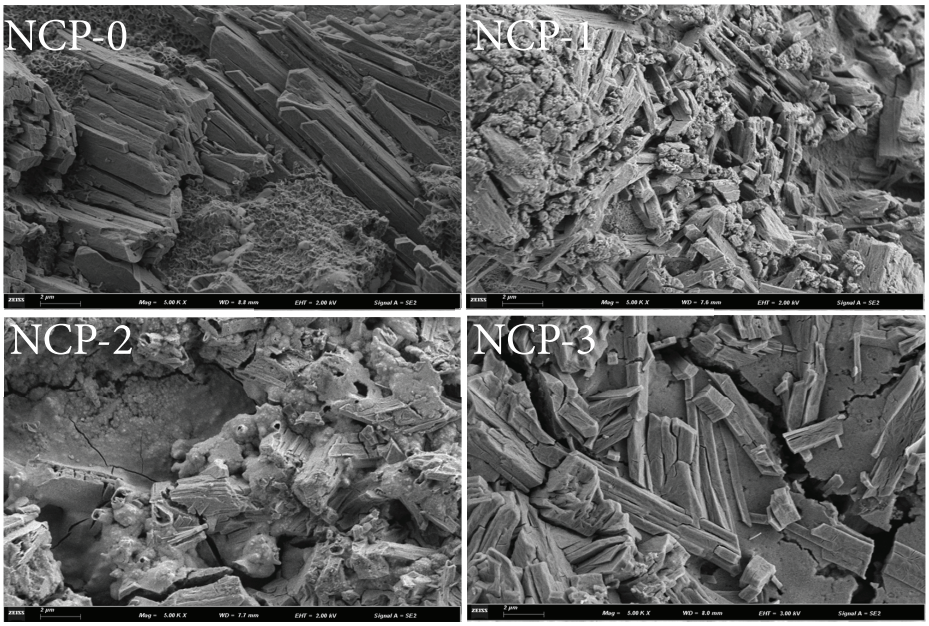

Figure 13 Microstructure of the passivation film on steel bars in MPC cementitious material under natural curing

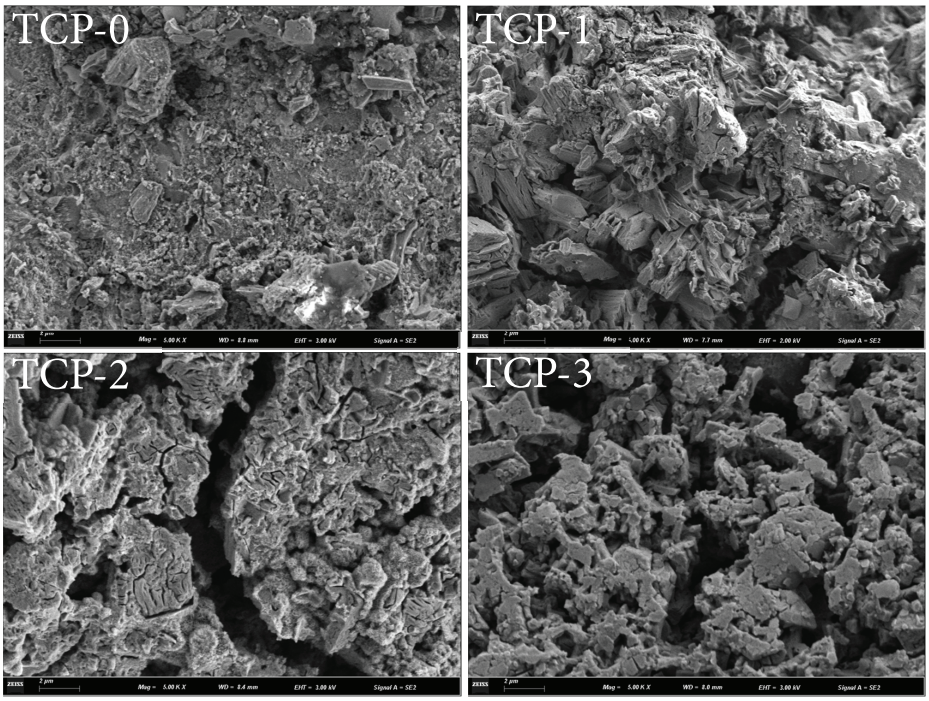

Figure 14 Microstructure of the passivation film on steel bars in MPC cementitious material under carbonation curing

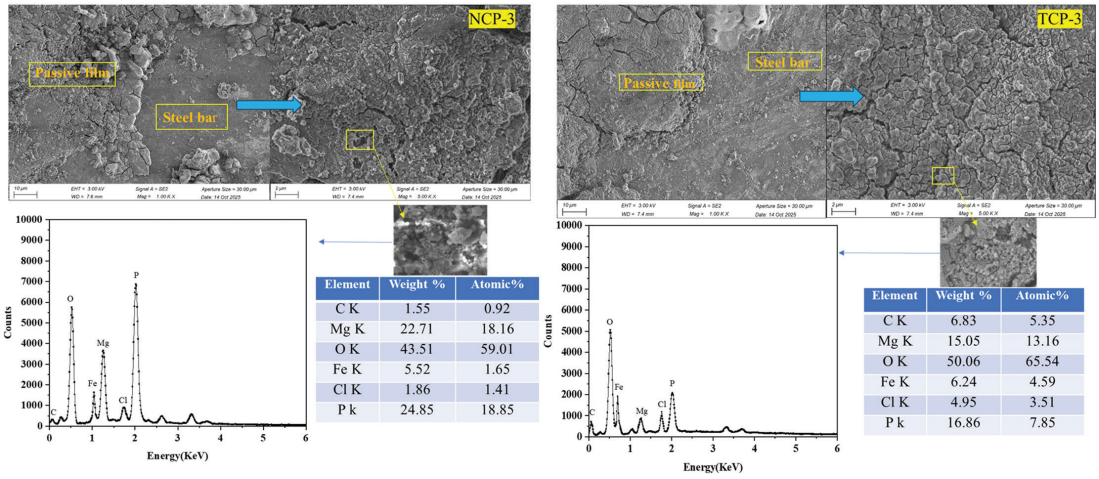

Figure 15 Micro-morphology and chemical composition of the passive film on the steel electrode surface

carbonation curing conditions, respectively. In the absence of chloride, a stable phosphate-type passive film forms on the steel surface. According to previous studies [33, 34], this film consists mainly of iron phosphates ($Fe_3(PO_4)_2$) and magnesium–potassium dihydrogen phosphate hydrate ($MgKH_2(PO_4)_2{\cdot}6H_2O$), which effectively suppress steel corrosion. As the chloride content increases, the film develops more surface pores, loses compactness, and exhibits exfoliation/delamination, leading to a significant reduction in corrosion-inhibiting capabilities. Under carbonation, the passive film further deteriorates, with the microstructure showing noticeable swelling and the formation of additional voids and cracks. EDS analyses (Figure 15) of NCP-3 and TCP-3 indicate that carbonation increases the C and Cl contents in the film. Taken together, these results suggest that carbonation promotes a transformation from phosphate phases—originally providing superior interfacial bonding to steel—to carbonate phases, facilitating the inward migration of chloride ions and undermining the stability and protective effectiveness of the film.

4 Conclusions

This study systematically evaluates the corrosion protection performance of magnesium phosphate cement (MPC) for steel reinforcement under chloride, carbonation, and their coupled action. The results indicate that chloride ingress significantly weakens the protective performance of MPC, with a critical chloride content of approximately 2% under natural curing, which decreases to about 1% under carbonation. Carbonation further intensifies chloride-induced corrosion, as reflected by the negative shift in open-circuit potential (OCP), the decrease in polarization/charge-transfer resistances, the increase in corrosion current I_{corr}, and the Warburg-type diffusion behavior revealed by low-frequency EIS under carbonation, indicating enhanced diffusion characteristics.

Microscopic analysis shows that under the coupled effect of chloride and CO_2, the original iron-phosphate-type passive film becomes more porous and cracked, leading to the degradation of the steel-to-matrix interfacial integrity. Corrosion tends to become more uniform, with pronounced end effects. In particular, carbonation induces a distinct transformation of the passive film, with phosphate-rich products gradually replaced by carbonate-containing phases, which further accelerates corrosion.

From an engineering perspective, MPC remains a promising binder for rapid repair and the protection of steel reinforcement. However, in environments containing both chloride and CO_2, the chloride content should be controlled below the identified thresholds (2% under natural curing and 1% under carbonation), and MPC should be used in conjunction with anti-carbonation measures, corrosion inhibitors, and enhanced interfacial protection strategies. These findings underscore the necessity of implementing integrated protective strategies to enhance the long-term durability of reinforced concrete structures exposed to chloride ingress and carbonation.

Acknowledgement

The authors gratefully acknowledge [Harbin Institute of Technology (Weihai) Qingdao Research Institute] for providing experimental facilities and technical support.

Funding Statement

This work was supported by the National Natural Science Foundation of China (NSFC) (Grant No. 52578296-LJZ). https://www.nsfc.gov.cn/.

Author Contributions

Hanxin Li: Investigation, Data curation, Formal analysis, Writing—original draft. Zhicheng Zhang: Validation, Writing—review & editing. Changkun

Song: Data curation, Visualization. Junzhe Liu: Methodology, Resources. Songyuan Ni: Conceptualization, Supervision, Funding acquisition, Writing—review & editing. All authors reviewed and approved the final version of the manuscript.

Availability of Data and Materials

The data that support the findings of this study are available in the article.

Ethics Approval

Not applicable.

Conflicts of Interest

The authors declare that they have no known competing financial interests or personal relationships that could have appeared to influence the work reported in this paper.

REFERENCES

[1] Liu S, Yang K, Yu L, Xu L, Yuan Q, Wu K, et al. Integrated assessment of magnesium phosphate cement repaired concrete from the perspective of mechanical, geometric and electrochemical compatibility. Cem Concr Compos. 2025;157:105958. doi:10.1016/j.cemconcomp.2025.105958.
[2] Zhang F. Corrosion resistance performance investigation of mild steel bar coated with magnesium phosphate cement paste [dissertation]. Rolla, MO, USA: Missouri University of Science and Technology; 2022.
[3] Wang D, Yue Y, Xie Z, Mi T, Yang S, McCague C, et al. Chloride-induced depassivation and corrosion of mild steel in magnesium potassium phosphate cement. Corros Sci. 2022;206:110482. doi:10.1016/j.corsci.2022.110482.
[4] Leng D, Fu Q, Ge Y, He C, Lv Y, Li X. Effect of K^+ diffusion on hydration of magnesium potassium phosphate cement with different Mg/P ratios: experiments and molecular dynamics simulation calculations. Materials. 2024;17(5):1151. doi:10.3390/ma17051151.
[5] Qin J, Qian J, You C, Fan Y, Li Z, Wang H. Bond behavior and interfacial micro-characteristics of magnesium phosphate cement onto old concrete substrate. Constr Build Mater. 2018;167:166–76. doi:10.1016/j.conbuildmat.2018.02.018.
[6] Sagar C, Chauhan A, Sharma UK. Synergistic effect of carbonation and cast-in-chlorides on corrosion initiation in reinforced concrete. Structures. 2025;72:108264. doi:10.1016/j.istruc.2025.108264.
[7] Mi T, Li Y, Liu W, Dong Z, Gong Q, Min C, et al. The effect of carbonation on chloride redistribution and corrosion of steel reinforcement. Constr Build Mater. 2023;363:129641. doi:10.1016/j.conbuildmat.2022.129641.
[8] Zeng Z, You J, Gu S, Wang J, Wei F, Xie X, et al. Study on passivation mechanism of HRB500E rebar in highly alkaline concrete pore solution. Sci Rep. 2025;15(1):29239. doi:10.1038/s41598-025-15606-4.
[9] Sun W, Liu C, Hong F, Wang P, Zhang Y, Wang X, et al. Deterioration of passivation film caused by carbonation in reinforced concrete: an electrochemical and nanoscale perspectives. J Build Eng. 2025;106:112524. doi:10.1016/j.jobe.2025.112524.
[10] Mundra S, Criado M, Bernal SA, Provis JL. Chloride-induced corrosion of steel rebars in simulated pore solutions of alkali-activated concretes. Cem Concr Res. 2017;100:385–97. doi:10.1016/j.cemconres.2017.08.006.
[11] Tian Y, Xu J, Shao Y, Zhang G, Yan D, Liu Y, et al. Dynamic analysis of chloride-induced passive film breakdown mechanisms in carbon steel within simulated concrete pore solution. Case Stud Constr Mater. 2025;22:e04409. doi:10.1016/j.cscm.2025.e04409.
[12] Zhang F, Qin J, Cai K, Myers JJ, Ma H. Anti-corrosion performance of magnesium potassium phosphate cement coating on steel reinforcement: the effect of boric acid. Materials. 2024;17(21):5310. doi:10.3390/ma17215310.
[13] Tang H, Qian J, Ji Z, Dai X, Li Z. The protective effect of magnesium phosphate cement on steel corrosion. Constr Build Mater. 2020;255(8):119422. doi:10.1016/j.conbuildmat.2020.119422.
[14] Tang H, Qian J, Qin J, Li Z, Jia X, Yue Y, et al. Electrochemical behavior of steel bars in magnesium phosphate cement. Cem Concr Res. 2023;169:107167. doi:10.1016/j.cemconres.2023.107167.
[15] Wang M, Ming X, Wang Q, Ding H, Dai Z, Tian L, et al. Environmentally friendly magnesium potassium phosphate cement-based coating with high anti-corrosion performance on iron. J Mater Res Technol. 2024;33:9951–9. doi:10.1016/j.jmrt.2024.11.220.
[16] Wang D, Yue Y, Qian J. Effect of carbonation on the corrosion behavior of steel rebar embedded in magnesium phosphate cement. Compos Part B Eng. 2024;268:111088. doi:10.1016/j.compositesb.2023.111088.
[17] Chen L, Su RKL. Corrosion rate measurement by using polarization resistance method for microcell and macrocell corrosion: theoretical analysis and experimental work with simulated concrete pore solution. Constr Build Mater. 2021;267:121003. doi:10.1016/j.conbuildmat.2020.121003.
[18] Sanni O, Iwarere SA, Daramola MO. Introduction: corrosion basics and corrosion testing. In: Electrochemical and analytical techniques for sustainable corrosion monitoring. Amsterdam, The Netherlands: Elsevier; 2023. p. 1–23. doi:10.1016/b978-0-443-15783-7.00015-3.
[19] Mei K, He Z, Yi B, Lin X, Wang J, Wang H, et al. Study on electrochemical characteristics of reinforced concrete corrosion under the action of carbonation and chloride. Case Stud Constr Mater. 2022;17(4):e01351. doi:10.1016/j.cscm.2022.e01351.
[20] Schiegg Y, Bisschop J, Von Greve-Dierfeld S. Monitoring steel bar corrosion propagation in concrete-results of the Naxberg field experiment after 12 years. In: European Corrosion Congress (EUROCORR 2017) and 20th International Corrosion Congress and Process Safety Congress 2017: Corrosion Control for Safer Living; 2017 Sep 3–7; Prague, Czech Republic. p. 1315.
[21] He D. Review of corrosion evaluation methods for steel reinforcement in concrete. Corros Mater Degrad. 2025;6(3):37. doi:10.3390/cmd6030037.
[22] Dabarera A, Fernández R, Provis JL. A systematic review of engineering properties of magnesium potassium phosphate cement as a repair material. Front Mater. 2024;11:1451079. doi:10.3389/fmats.2024.1451079.
[23] Li MLL, Kee SH, Monjardin CEF, Robles KPV. Numerical and experimental correlation between half-cell potential and steel mass loss in corroded reinforced concrete. Materials. 2025;18(22):5238. doi:10.3390/ma18225238.
[24] ASTM C876-15. Standard test method for corrosion potentials of uncoated reinforcing steel in concrete. West Conshohocken, PA, USA: ASTM International; 2015. 7 p.
[25] Rodrigues R, Gaboreau S, Gance J, Ignatiadis I, Betelu S. Reinforced concrete structures: a review of corrosion mechanisms and advances in electrical methods for corrosion monitoring. Constr Build Mater. 2021;269:121240. doi:10.1016/j.conbuildmat.2020.121240.
[26] Zhao S, Zhang D, Li Y, Gao H, Meng X. Physical and mechanical properties of novel porous ecological concrete based on magnesium phosphate cement. Materials. 2022;15(21):7521. doi:10.3390/ma15217521.
[27] Yodsudjai W, Pattarakittam T. Factors influencing half-cell potential measurement and its relationship with corrosion level. Measurement. 2017;104(1):159–68. doi:10.1016/j.measurement.2017.03.027.
[28] Ma H, Li Z, Chen E, Yu H, Tan Y, Wu C, et al. Research on the corrosion behavior of rebar in basic magnesium sulfate cement concrete based on the electrochemical impedance spectroscopy method. Constr Build Mater. 2025;466:140326. doi:10.1016/j.conbuildmat.2025.140326.
[29] Zhang L, Liu G, Yang L, Zhang Y. Experimental and ReaxFF MD study on Cr10Mo steel passivation in simulated concrete pore solutions. Case Stud Constr Mater. 2024;21:e03752. doi:10.1016/j.cscm.2024.e03752.
[30] Ali M, Shams MA, Bheel N, Almaliki AH, Mahmoud AS, Dodo YA, et al. A review on chloride induced corrosion in reinforced concrete structures: lab and *in situ* investigation. RSC Adv. 2024;14(50):37252–71. doi:10.1039/d4ra05506c.
[31] Chen M, Liu X, Mei K, Wang S, Liu J, Li Y. Corrosion behavior of steel bar in magnesium oxysulfide cement-based materials: the role of chloride and nitrite. J Mater Res Technol. 2024;32:1577–88. doi:10.1016/j.jmrt.2024.08.020.
[32] Lu Q, Wang L, Xin J, Tian H, Wang X, Cui Z. Corrosion evolution and stress corrosion cracking of E690 steel for marine construction in artificial seawater under potentiostatic anodic polarization. Constr Build Mater. 2020;238:117763. doi:10.1016/j.conbuildmat.2019.117763.
[33] Zhang J, Niu W, Liu Z, Yang Y, Long W, Zhang Y, et al. Hydration behavior of magnesium potassium phosphate cement: experimental study and thermodynamic modeling. Materials. 2022;15(23):8496. doi:10.3390/ma15238496.
[34] Le Rouzic M, Chaussadent T, Platret G, Stefan L. Mechanisms of k-struvite formation in magnesium phosphate cements. Cem Concr Res. 2017;91:117–22. doi:10.1016/j.cemconres.2016.11.008.